

# Molecular dynamics simulation of water permeation through the alpha-hemolysin channel

Jirasak Wong-ekkabut<sup>1</sup> · Mikko Karttunen<sup>2,3</sup>

Received: 14 January 2015 / Accepted: 21 July 2015 / Published online: 12 August 2015  
© Springer Science+Business Media Dordrecht 2015

**Abstract** The alpha-hemolysin (AHL) nanochannel is a non-selective channel that allows for uncontrolled transport of small molecules across membranes leading to cell death. Although it is a bacterial toxin, it has promising applications, ranging from drug delivery systems to nano-sensing devices. This study focuses on the transport of water molecules through an AHL nanochannel using molecular dynamics (MD) simulations. Our results show that AHL can quickly transport water across membranes. The first-passage time approach was used to estimate the diffusion coefficient and the mean exit time. To study the energetics of transport, the potential of mean force (PMF) of a water molecule along the AHL nanochannel was calculated. The results show that the energy barriers of water permeation across a nanopore are always positive along the channel and the values are close to thermal energy ( $k_B T$ ). These findings suggest that the observed quick permeation of water is due to small energy barriers and a hydrophobic inner channel surface resulting in smaller friction. We speculate that these physical mechanisms are important in how AHL causes cell death.

**Keywords** Alpha hemolysin · Molecular dynamics simulations · Water permeation · Biological membrane · Lipid bilayer

---

✉ Jirasak Wong-ekkabut  
jirasak.w@ku.ac.th

✉ Mikko Karttunen  
mkarttu@gmail.com

<sup>1</sup> Department of Physics, Faculty of Science, Kasetsart University, 50 Phahon Yothin Rd, Chatuchak, Bangkok, Thailand 10900

<sup>2</sup> Department of Chemistry and Waterloo Institute for Nanotechnology, University of Waterloo, 200 University Avenue West, Waterloo, Ontario, Canada N2L 3G1

<sup>3</sup> Department of Mathematics and Computer Science & Institute for Complex Molecular Systems, Eindhoven University of Technology, PO Box 513, MetaForum, 5600 MB Eindhoven, The Netherlands

## 1 Introduction

Alpha-hemolysin (AHL) is a bacterial toxin, secreted by the human pathogen *Staphylococcus aureus* [1]. It has a heptameric structure consisting in 33.2-kDa water-soluble monomers that self-assemble to form a 232.4-kDa transmembrane pore [2]. High-resolution X-ray crystallography [3] shows that the protein has a mushroom shape and is about 10 nm in height (Fig. 1). The main structure consists in a cap and beta-barrel stem. The largest diameter inside is about 4.6 nm and located in the cap. The narrowest part is in the stem with a diameter of about 1.6 nm (Fig. 2) [4–6]. The protein pore is fully occupied by ~1500 water molecules. The water density in the cap region is close to the bulk density of water but in the stem the density is significantly lower. There are two density minima [5, 7, 6] in the stem:  $548 \pm 93 \text{ kg/m}^3$  and  $526 \pm 86 \text{ kg/m}^3$ , which are the locations of the hydrophobic residues, leucine (Leu135, Leu428, Leu721, Leu1014, Leu1307, Leu1600 and Leu1893) and methionine (Met113, Met406, Met699, Met992, Met1285, Met1578 and Met1871), respectively. The pore is non-selective and thus allows for transport of water, ions, and small molecules. This may lead to rapid osmotic swelling and cell death [8, 9].

The non-selective nature of transport is appealing for applications in nanotechnology and medicine [10–12]. For example, one could bombard cancer cells with proteins that would damage cells' outer membranes, making them susceptible to chemotherapy [13, 14]. It may also be possible to make artificial pores, embed them into membranes, and use them as biosensors [15, 16, 12, 17]. However, permeation of small molecules across AHL is not fully understood. Few studies have focused on the transportation of ions through AHL. They found that the wild-type channel shows weak anion conductivity [5, 18, 19] and site-directed mutations at the constriction region inside the channel [20, 21, 18], such as K147N or M113P, can be made to tune the channel to be moderately cation selective. The transport of water and small molecules plays a key role in biological activities and there have been several studies focusing on aquaporin [22–24] and carbon nanotubes [25, 26]. Interestingly, it has also been reported that a single file water structure and long-lasting hydrogen bonds in confined geometry result in faster transportation of water [27, 28]. Working with a bigger pore but still

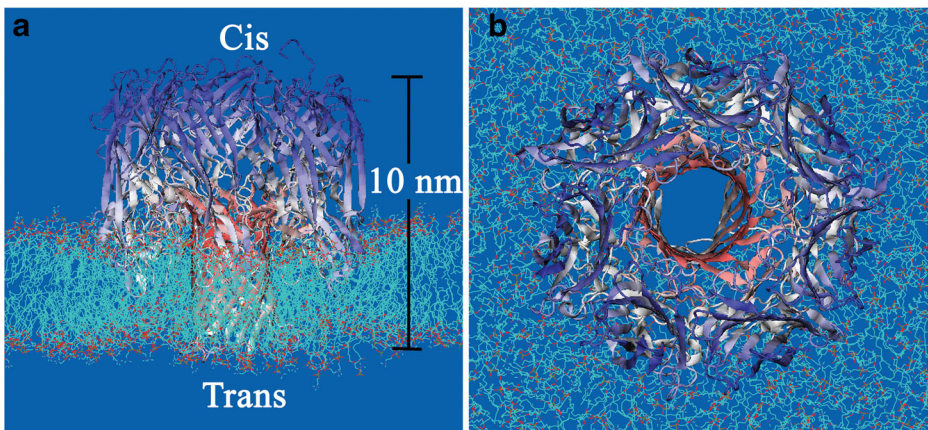


**Fig. 1** Snapshots from a simulation after 80 ns: side view (a) and top view (b). The protein is embedded in a POPC lipid bilayer. Water molecules hydrate the system and occupy the protein pore (water molecules were omitted from the visualization for clarity)

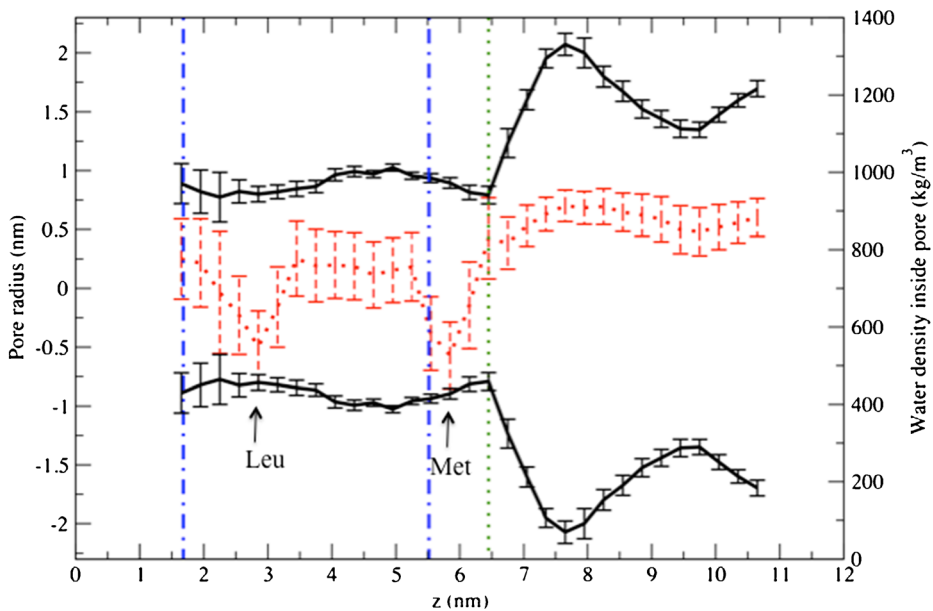


**Fig. 2** Pore radius is represented by the solid black line and water density inside it is shown by the red dotted line. The blue dot-dashed lines represent the average phosphate locations of the lipids in the lipid bilayer. The constriction (the narrowest pore radius) is indicated by the green dotted line. The results are based on an 80-ns production simulation and the error bars are given by standard deviation over simulation time. The density minima in the stem are located at  $z=2.9$  and  $5.9$  nm corresponding to the locations of the hydrophobic residues, Leucine (Leu135, Leu428, Leu721, Leu1014, Leu1307, Leu1600 and Leu1893) and Methionine (Met113, Met406, Met699, Met992, Met1285, Met1578 and Met1871), respectively

in nanoscale, Cisse et al. [29] created porous lipid nanocontainers by incorporating a channel protein. This introduces permanent pores into synthetic lipid vesicles and enables exchange with a bulk solution.

Both experimental and theoretical approaches have been used to investigate the mechanisms of molecular transport [22, 23, 30, 25, 31–33]. At the microscopic level, experiments have reached the resolution limit, creating the need for MD simulations. For example, using atomistic MD, Hummer et al. [25] predicted that a hydrophobic carbon nanotube can be filled by water and transport water. This prediction was confirmed by experiments 5 years later [30].

MD simulation is a powerful technique but transport through nanoscale tubes and channels poses significant challenges. In particular, several error sources have been discovered by a number of groups [31, 34, 35]. For example, Ni et al. [34] performed MD simulations of protein human interleukin-4 and a short DNA fragment in explicit water and they found that the inappropriate treatment of electrostatic interactions produces artificial repulsion between charged residues. This was identified as the reason behind the artificial unfolding of proteins in MD simulation [34]. Other examples relevant to water transport include Gong et al. [36], who reported the spontaneous and continuous unidirectional flow of water through an asymmetrical charged nanotube. Unfortunately, the unidirectional flow in their simulations was the result of a combination of artifacts from using improper charge groups, thermostatting and update frequency of long-range interactions [6, 35].

In this study, we focus on permeation mechanisms of water through AHL. The results show that AHLs are capable of transporting water molecules with high permeability compared to

other water channels such as aquaporin (AQP). The potential of the mean force indicated that the energy barrier of water transport across the channel is of the order  $k_B T$ . Our study suggests that the fast transport of water through an AHL channel causes uncontrollable molecular exchange across a cell membrane and may lead to cell death.

## 2 Molecular dynamics (MD) simulations

Classical MD simulations of AHL [3] embedded into a palmitoyl oleoyl phosphatidylcholine (POPC) lipid bilayer [37] to study permeation of water into the protein pore (Fig. 1) were performed. The AHL structure was taken from the protein data bank (PDB ID 7AHL) [3, 38] and the GROMOS force-field [39] was used.

AHL is protonated at neutral pH [40], resulting in a positively (+7e) charged structure. To maintain overall charge neutrality, 7  $\text{Cl}^-$  counter-ions were added. A pre-equilibrated POPC lipid bilayer structure was used [41]. The double bonds of POPC lipids were modeled using the corrections of Bachar et al. [42, 43]. The system consisted in one AHL, 401 POPC lipids, 7  $\text{Cl}^-$  counter-ions and 36,747 water molecules. Water was modeled using the simple point charge model (SPC) [44]. The simulation box size was 12.9 nm  $\times$  12.8 nm  $\times$  12.0 nm. After energy minimization using the steepest decent method to remove cavities and close contacts, a 100-ns equilibration run was performed. This was followed by 80-ns production runs of three independent systems to ensure that there is no dependence on initial conditions. The simulations were carried out with the GROMACS package version 4.0.5 [45] in the NVT (constant particle number, volume, and temperature) ensemble. The integration time step was set to 1 fs. The trajectories and forces were saved every 2 ps for analysis. Periodic boundary conditions were applied in all directions. Protein, lipids, and water molecules were thermostated separately at a temperature of 323 K. Parameters and protocol established in previous works [6, 35] were used: V-rescale thermostat [46, 47], Particle Mesh Ewald (PME) [48–50] and neighbor list update at each time step [6, 35]. Visualizations were done using Visual Molecular Dynamics (VMD) software [51].

## 3 Simulation results and discussions

### 3.1 Permeation of water and potential of mean force along the channel

The fully occupied AHL channel contains  $1479 \pm 32$  water molecules. During the 80-ns production simulations (Fig. 3),  $2410 \pm 48$  water molecules moved from *cis* to *trans* (the same direction as in transport into the cell) and  $2402 \pm 108$  water molecules in the opposite direction: the rate of transport ( $R_t$ ) across the AHL channel was around 66 molecules/ns without preferential direction (i.e., zero net flux) (Fig. 3). This rate is about three times faster than the transport of water molecules through a single-walled carbon nanotube ( $\sim 17$  molecules/ns) with the dimensions of 1.34 nm in length and 0.81 nm in diameter [25] and about an order of magnitude higher than the bacterial glycerol facilitator GlpF ( $R_t$  reported by experimental and computational studies were 0.5 and 1.0 molecules/ns [52, 22], respectively). From the transport rate of water through AHL, we obtain a permeability ( $p_f$ ) of  $1.9 \times 10^{-12}$   $\text{cm}^3/\text{s}$ . ( $p_f = \nu_w R_t / N_A$  where  $\nu_w$  is the average volume of a single water molecule, 18  $\text{cm}^3/\text{mol}$ ,  $R_t$  is the rate of water transport across the channel and  $N_A$  is Avogadro's number). This is in good agreement with both computational and experimental studies [5, 53]: Aksimentiev et al. [5]

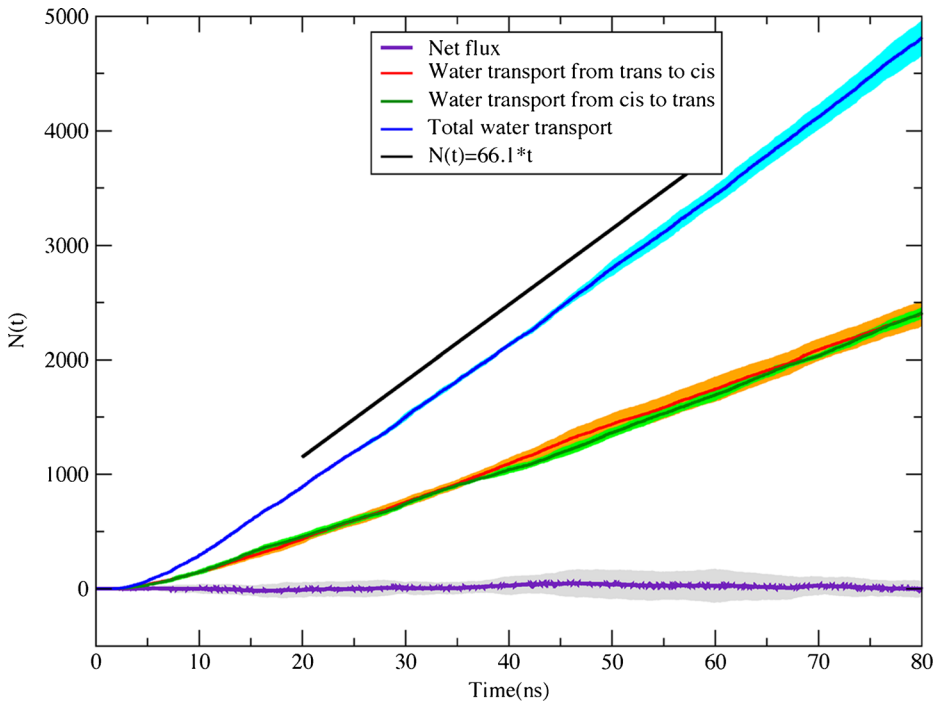


**Fig. 3** The number of water molecules transported through the nanopore as a function of time (blue line). After 80 ns,  $2410 \pm 48$  and  $2402 \pm 108$  water molecules were transported from *cis* to *trans* (green line) and vice versa (red line), respectively. The rate of water transport across the AHL pore was 66 molecules/ns (black line) with no preferential flow direction (purple line). The net flux is defined as the difference of the number of water molecules transported from *cis* to *trans* and vice versa. The broad light grey, orange, green, and blue lines represent the standard deviation of net flux, transport from *trans* to *cis* and transport from *cis* to *trans* and total water transport, respectively

obtained  $p_f = 1.9 \times 10^{-12} \text{ cm}^3/\text{s}$  after the low viscosity of the TIP3P water model was taken into account [54]. Although the different water models give quantitatively different values for transport coefficients, transport properties and conversion factors have been extensively studied and documented and between the most common water models there are no major qualitative differences provided one is far away from phase transitions, as is the case here [55–57]. Experimentally, the average permeability of a single AHL channel for water has been found to be in the range between  $1.3 \times 10^{-12}$  and  $1.5 \times 10^{-12} \text{ cm}^3/\text{s}$ , depending on the pH [53].

In comparison with other protein channels, the permeability of AHL is an order of magnitude higher than a water channel such as aquaporin-1 ( $p_f = 0.6\text{--}1.1 \times 10^{-13} \text{ cm}^3/\text{s}$ ) and aquaporin-4 ( $p_f = 2.4 \times 10^{-13} \text{ cm}^3/\text{s}$ ) [58, 59] but it is in the same order of magnitude as desformylgramicidin ( $p_f = 1.1 \times 10^{-12} \text{ cm}^3/\text{s}$ ) [60] and the *Streptomyces lividans*  $\text{K}^+$  (KcsA) channel ( $p_f = 4.8 \times 10^{-12} \text{ cm}^3/\text{s}$ ) [61]. Although the mobility of water to transport through AHL and KcsA is equivalently fast, the mechanism may not be completely the same. The fast transport of water through KcsA was consistent with liquid-vapor oscillation [26, 61], which can occur due to geometrical confinement of water in the hydrophobic nanochannel. On the other hand, AHLs have hydrophobic residues especially on the surface inside the channel. The pore is, however, always occupied by water because the pore's diameter is about 60% larger than that of KcsA (the narrowest diameters of AHL [3–6] and KcsA [62, 63] are 1.6 and 1.0 nm, respectively).

Transport of water molecules across different nanochannels has been intensely studied by MD simulations [24, 26, 64–67]. Next, we focus on the dynamical properties of water molecules, in particular the first-passage time and diffusion coefficient. The first-passage time [68–70] is the residence time of a molecule passing through the channel. It is determined by measuring the permeation time of molecules entering the channel at one side and leaving it at the other. The distribution of the passage time has been used for characterizing the diffusive properties through heterogeneous channels. Van Hijkoop et al. [69] successfully analyzed water diffusing through carbon nanotubes and OmpF channels. The normalized distribution of the passage time of water in the AHL nanochannel,  $F_p(t)$ , is shown in Fig. 4 and fitted to Eq. (1) [69]:

$$F_p(t) = \frac{2\pi^2 D}{L^2} \sum_{n=1}^{\infty} (-1)^{n-1} n^2 e^{-t/\tau_n} \tag{1}$$

where  $L$  is channel length,  $D$  is the diffusion coefficient and the time constants  $\tau_n$  are defined as  $\tau_n = \frac{L^2}{n^2 \pi^2 D}$ . Following van Hijkoop et al., we also computed the survival probability  $S_p(t)$ . It gives the proportion of molecules that remain in the channel after time  $t$ .  $S_p(t)$  is determined by integrating Eq. (1):

$$S_p(t) = \int_t^{\infty} F_p(t') dt' = 2 \sum_{n=1}^{\infty} (-1)^{n-1} e^{-t/\tau_n} \tag{2}$$

$S_p(t)$  can be used to determine if instead of only one ( $n=1$ ) several diffusion modes are present.

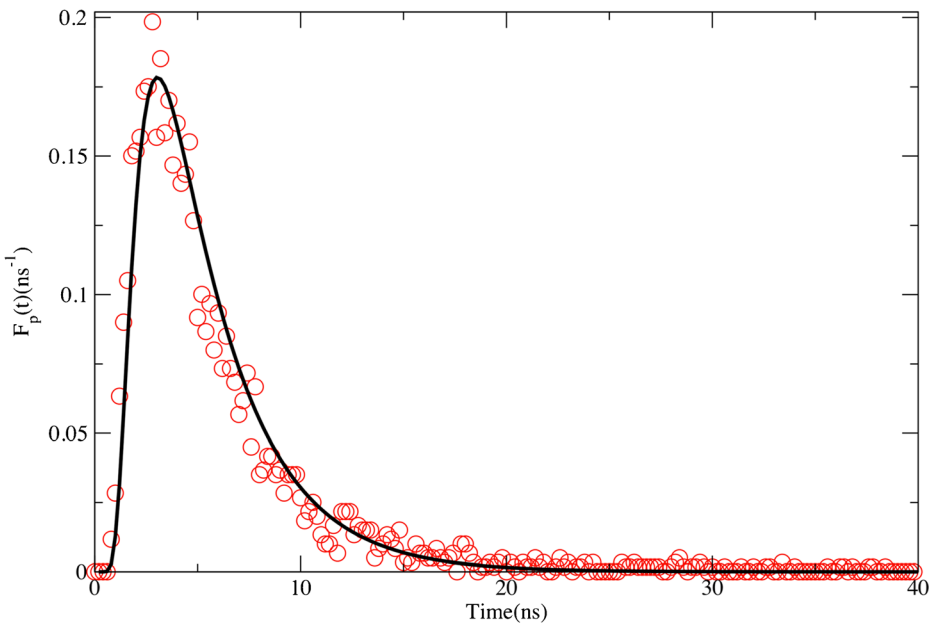


**Fig. 4** The normalized distribution of the first-passage times of water molecules transported across the AHL channel. *Circles*: simulation data. *Black line*: fit to  $F_p(t)$ , Eq. (1)

We found that the diffusion coefficient ( $D$ ) was  $2.67 \pm 0.05 \text{ nm}^2/\text{ns}$  and the spatially averaged mean exit time ( $\langle T \rangle = \frac{L^2}{12D}$ ) was  $2.71 \pm 0.05 \text{ ns}$ . The mean exit times were the same in both directions (*cis* to *trans* and vice versa). In comparison to other channels, the diffusion coefficients of water in a carbon nanotube with a diameter of 1.2 nm and an OmpF channel were  $D=2.70 \text{ nm}^2/\text{ns}$  and  $1.60 \text{ nm}^2/\text{ns}$  [69], respectively. The water molecule diffusion through the AHL channel is as fast as the one through carbon nanotubes [71, 69] and almost two-times faster than through the OmpF channel [69]. This fast transport of water might be related to the pore size of AHL and the hydrophobicity of the inner surface along the channel [28]. However, care must be taken when comparing different studies because the properties of water models may have some influence on the results. For example, the SPC/E model was used by Mashl et al. [71] and van Hijkoop et al. [69], as well as in a model of modified SPC water [72] in which the diffusion coefficient of their model appears to be reduced by 15% relative to the regular SPC water model [73].

The diffusion coefficient of water inside the channel was also determined by mean square displacement (MSD) (Fig. 5). MSD shows two regimes, ballistic and diffusive with  $D_1=2.92 \pm 0.02$  and  $D_2=0.20 \pm 0.01 \text{ nm}^2/\text{ns}$ , respectively.  $D_1$  is slightly higher than the value obtained from the first-passage time although very close. Diffusion in narrow channels depends strongly on the width and structure of the channel as discussed by Striolo [74]. Both Striolo and van Hijkoop et al. [69] found behavior similar to ours, that is, ballistic and diffusive regimes and first-passage time give a value that is close to the ballistic one. We examined this also by computing  $S_p(t)$  using Eq. (2) (inset in Fig. 5). Both the MSD and  $S_p(t)$  show the two regimes.

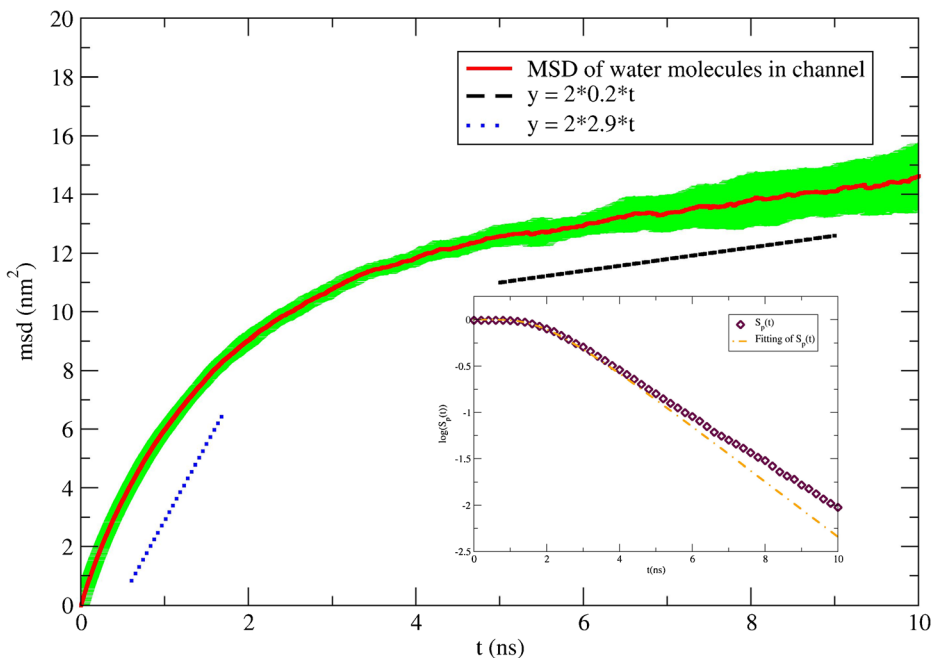


**Fig. 5** The mean square displacement (MSD) of water molecules inside the channel (red line). Two regimes, ballistic and diffusive, are present with diffusion coefficients of  $D_1=2.92 \pm 0.02$  (blue dots) and  $D_2=0.20 \pm 0.01$  (black dashed line)  $\text{nm}^2/\text{ns}$ , respectively. The broad light green line represents the standard deviation of MSD averaged over the three systems. The inset shows the survival probability (diamonds) and a fit to  $S_p(t)$  (orange dot-dashed line), Eq. (2)

Examination of the trajectories showed that this is most likely due to a population of water molecules that are hydrogen bonded to the channel walls for a longer time. This issue will be addressed in more detail in a separate study.

Finally, Fig. 5 shows the MSD up to 10 ns. Due to a finite length of the channel, MSD shows saturation at longer time scales similar to that discussed by Mukherjee et al. [75] in the context of carbon nanotubes. Due to the presence of an internal reservoir of water molecules in the vestibule region of the AHL, reaching saturation takes much longer than in narrow carbon nanotubes. Saturation occurred roughly at around 25 ns but data are not shown in Fig. 5 due to lack of statistics and hence large error bars.

To understand the energetics of water transport through the AHL channel, the forces acting on water molecules along the  $z$ -direction were calculated. The slabs of water molecules were divided along the  $z$ -axis with a thickness of 0.3 nm and only the water molecules inside the AHL channel were considered. The forces acting on water molecules were averaged over 80 ns and are shown in Fig. 6. The strongest force acting on the water molecules was found to be  $3.39 \pm 0.25$  kJ/(mol nm) in the  $-z$ -direction at  $z=5.6$  nm. This position corresponds to the hydrophobic region of methionine (Met) residues (Met113, Met406, Met699, Met992, Met1285, Met1578 and Met1871). The potential of mean force (PMF) is calculated by integrating the averaged forces along the  $z$ -direction [76–78] using:

$$W = - \int_0^z \langle f(z) \rangle dz \quad (3)$$

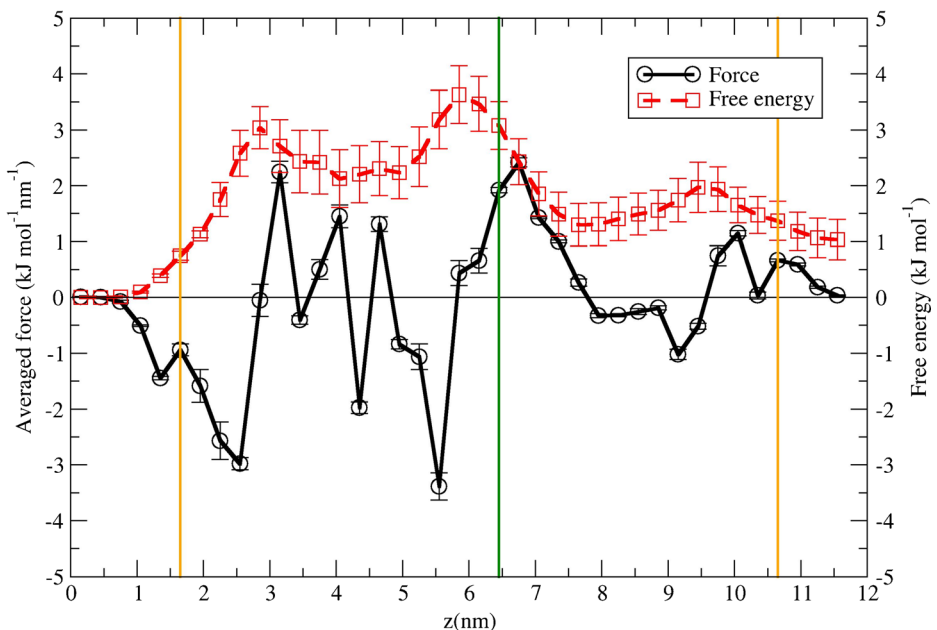


**Fig. 6** The averaged forces acting on water molecules and the potential of mean force (PMF) along the channel in the  $z$ -direction. The plots were averaged from three trajectories with a simulation time of 240 ns in total. The error bars were calculated by the standard deviation. The orange vertical lines represent the pore ends ( $z=1.7$  and  $10.7$  nm) and the green line represents the pore constriction ( $z=6.5$  nm)

The PMF profile is always positive along the channel as implied by hydrophobicity of the channel (Fig. 6). The PMF profile consists in three potential barriers along the channel: two peaks in the stem region at  $z=2.9$  nm (Leu135, Leu428, Leu721, Leu1014, Leu1307, Leu1600 and Leu1893) and 5.9 nm (Met113, Met406, Met699, Met992, Met1285, Met1578 and Met1871) and one peak in the cap region at  $z=9.5$  nm (Ile7, Ile300, Ile593, Ile886, Ile1179, Ile1472 and Ile1765). All peaks correspond to hydrophobic amino acid residues, leucine, methionine, and isoleucine. The largest energy barrier was at the constriction region with a value of  $3.6 \pm 0.5$  kJ/mol at  $z=5.9$  nm. The energy barriers are comparable to thermal energy ( $k_B T$  is about 2.69 kJ/mol at 323 K). The free energies at the pore ends of both sides were almost the same with values of around 1 kJ/mol. Figure 7 shows that at the ends, the number of hydrogen bonds per molecule approaches its bulk value and its lowest value at the constriction region. The number of H-bonds per molecule in the channel is also clearly smaller than in the vestibule contributing to both transport and barriers. To verify the PMF profile, additional Langevin dynamics (LD) simulations were performed with an inverse friction constant of 0.1 ps for 50 ns and the PMF profile was calculated by using Eq. (3). The result is in agreement with the MD simulation; the energy difference between LD and MD simulations was less than 1 kJ/mol (Fig. 8). To compare our PMF profile with the other techniques of PMF calculation [22, 79], we analyzed the PMF profile for water permeating through the AHL using:

$$G_{PMF}(z) = -k_B T \ln \left[ \frac{\rho(z)}{\rho_0} \right] \quad (4)$$

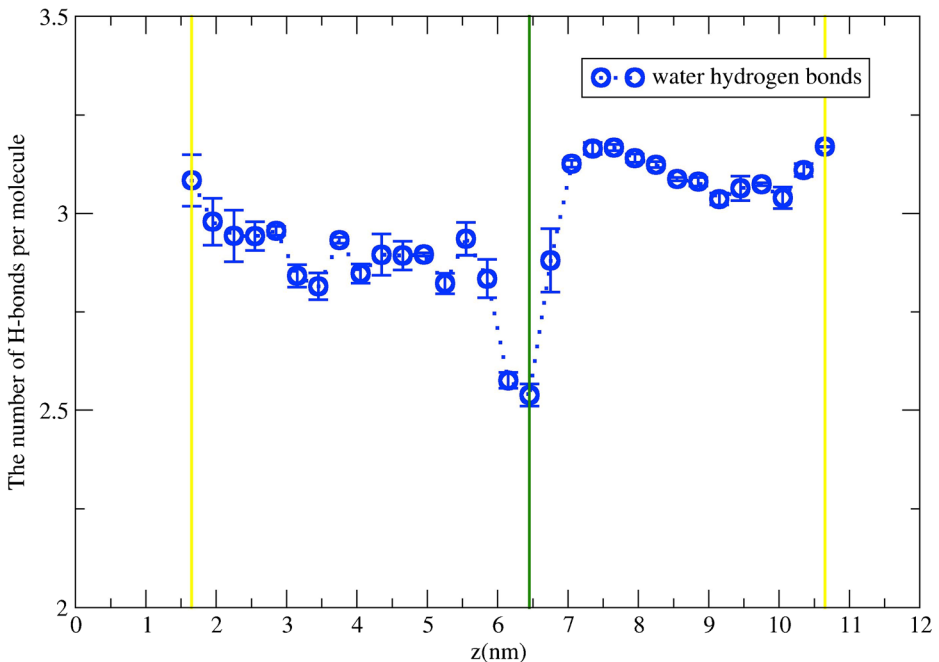


**Fig. 7** The number of H-bonds per water molecule inside the channel along the  $z$ -direction. The plots were averaged from three trajectories over 240 ns. The error bars represent standard deviation. The orange vertical lines show the pore ends ( $z=1.7$  and  $10.7$  nm) and the green lines the pore constriction ( $z=6.5$  nm)

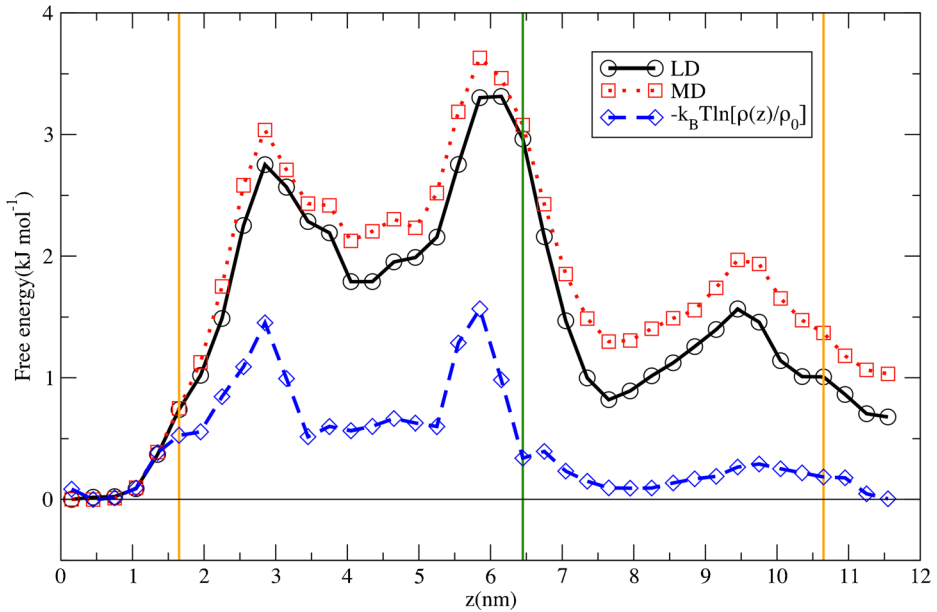


**Fig. 8** The potential of mean force (PMF) along the channel in the  $z$ -direction. The *black circles* and *red squares* represent the PMF profiles determined from MD and LD simulations using Eq. (3). The *blue diamonds* show the PMF determined using Eq. (4) in which the water density was determined from MD simulations. The *orange dotted vertical lines* represent the pore ends ( $z=1.7$  and  $10.7$  nm) and the *green dotted line* represents the pore constriction ( $z=6.5$  nm)

where  $\rho(z)$  is the water density along the channel and  $\rho_0$  is the bulk water density. The bulk water density in our simulation was determined to be  $943 \text{ kg/m}^3$ , which is similar to previous studies of SPC water density of  $962 \text{ kg/m}^3$  at  $323 \text{ K}$  [80, 81]. The results show that the values using this method are consistently smaller (the difference was up to  $2 \text{ kJ/mol}$ ). Although we cannot test this conclusively in this study, the difference may be due to a force field; the average absolute errors of the solvation free energy of amino acids when compared to experiment are  $5.1 \text{ kJ/mol}$  (AMBER),  $4.4 \text{ kJ/mol}$  (CHARMM),  $3.1 \text{ kJ/mol}$  (OPLS-AA), and  $0.9 \text{ kJ/mol}$  (GROMOS) [82, 39]. Despite the values of energy, the qualitative PMF profiles are similar (Fig. 8). In particular, the positions of all peaks are the same. In summary, the small energy barrier in the AHL channel allows for water transport with less friction resulting in fast transport across the AHL in comparison with other channels [22, 52, 69, 79]. This is a major function of the AHL channel to kill cells [8, 9].

## 4 Conclusions

In this work, we performed MD simulations to study water permeation through an AHL nanochannel embedded in a lipid bilayer. The potential of mean force (PMF) profile of water transported across the AHL nanochannel was determined and verified by several methods. The results showed that the free energy barriers are positive and of the same magnitude as thermal energy. This allows for water molecules to be easily transported across the AHL nanochannel. Based on this observation, we suggest that the fast transport of water molecules across this

channel is primarily due to low energy barriers. In addition, the hydrophobic residues on the inner pore's surface may contribute to the observed fast transport. Fast transport of water molecules by the AHL nanochannel causes uncontrolled molecular concentration inside the cell. Water is the basic molecule in all systems and the AHL channel has been adopted for, e.g., stochastic sensing [12, 83–85]. The results on water permeation through the AHL channel provide fundamental information that can be used in future studies of more complex and larger molecules such as ions, RNA, DNA, etc. [17, 19, 86–88]

**Acknowledgments** We thank Dr. Saree Phongphanphanee (Department of Materials Science, Faculty of Science, Kasetsart University) for helpful discussions. Financial support was provided by the Kasetsart University Research and Development Institute (KURDI) [JW], the Faculty of Science at Kasetsart University [JW], the Graduate School at Kasetsart University [JW] and the Asia Research Center (ARC) at Chulalongkorn University [JW]. Computational resources were provided by SHARCNET ([www.sharcnet.ca](http://www.sharcnet.ca)), Compute Canada and the Department of Physics, Faculty of Science, Kasetsart University.

## References

1. Dinges, M.M., Orwin, P.M., Schlievert, P.M.: Exotoxins of *Staphylococcus aureus*. Clin. Microbiol. Rev. **13**(1), 16–34 (2000)
2. Xiong, Y.Q., Willard, J., Yeaman, M.R., Cheung, A.L., Bayer, A.S.: Regulation of *Staphylococcus aureus* alpha-toxin gene (*hla*) expression by *agr*, *sarA*, and *sae* in vitro and in experimental infective endocarditis. J. Infect. Dis. **194**(9), 1267–1275 (2006)
3. Song, L.Z., Hobaugh, M.R., Shustak, C., Cheley, S., Bayley, H., Gouaux, J.E.: Structure of staphylococcal alpha-hemolysin, a heptameric transmembrane pore. Science **274**(5294), 1859–1866 (1996)
4. Gouaux, E.: Alpha-hemolysin from *Staphylococcus aureus*: an archetype of beta-barrel, channel-forming toxins. J. Struct. Biol. **121**(2), 110–122 (1998)
5. Aksimentiev, A., Schulten, K.: Imaging alpha-hemolysin with molecular dynamics: ionic conductance, osmotic permeability, and the electrostatic potential map. Biophys. J. **88**(6), 3745–3761 (2005)
6. Wong-ekkabut, J., Karttunen, M.: Assessment of common simulation protocols for simulations of nanopores, membrane proteins, and channels. J. Chem. Theor. Comput. **8**(8), 2905–2911 (2012)
7. Cozmuta, I., O’Keeffe, J.T., Bose, D., Stole, V.: Hybrid MD-Nernst Planck model of alpha-hemolysin conductance properties. Mol. Simul. **31**(2-3), 79–93 (2005)
8. Alouf, J.E., Freer, J.H.: The comprehensive sourcebook of bacterial protein toxins, 2nd edn. Academic Press, London (1999)
9. Menestrina, G., Dalla Serra, M., Prevost, G.: Mode of action of beta-barrel pore-forming toxins of the staphylococcal alpha-hemolysin family. Toxicon **39**(11), 1661–1672 (2001)
10. Bayley, H.: Pore-forming proteins with built-in triggers and switches. Bioorg. Chem. **23**(4), 340–354 (1995)
11. Bayley, H.: Building doors into cells. Sci. Am. **277**(3), 62–67 (1997)
12. Wanunu, M.: Nanopores: a journey towards DNA sequencing. Phys. Life Rev. **9**(2), 125–158 (2012)
13. Panchal, R.G., Cusack, E., Cheley, S., Bayley, H.: Tumor protease-activated, pore-forming toxins from a combinatorial library. Nature Biotech. **14**(7), 852–856 (1996)
14. St Jean, A.T., Swofford, C.A., Panteli, J.T., Brentzel, Z.J., Forbes, N.S.: Bacterial delivery of *Staphylococcus aureus* alpha-hemolysin causes regression and necrosis in murine tumors. Mol. Ther. **22**(7), 1266–1274 (2014)
15. Nakane, J., Wiggin, M., Marziali, A.: A nanosensor for transmembrane capture and identification of single nucleic acid molecules. Biophys. J. **87**(1), 615–621 (2004)
16. Maglia, G., Restrepo, M.R., Mikhailova, E., Bayley, H.: Enhanced translocation of single DNA molecules through alpha-hemolysin nanopores by manipulation of internal charge. Proc. Natl. Acad. Sci. U. S. A. **105**(50), 19720–19725 (2008)
17. Ivankin, A., Henley, R.Y., Larkin, J., Carson, S., Toscano, M.L., Wanunu, M.: Label-free optical detection of biomolecular translocation through nanopore arrays. ACS Nano **8**(10), 10774–10781 (2014)
18. Noskov, S.Y., Im, W., Roux, B.: Ion permeation through the alpha-hemolysin channel: theoretical studies based on Brownian dynamics and Poisson-Nernst-Planck electrodiffusion theory. Biophys. J. **87**(4), 2299–2309 (2004)

19. Bhattacharya, S., Muzard, L., Payet, L., Mathe, J., Bockelmann, U., Aksimentiev, A., Viasnoff, V.: Rectification of the current in alpha-hemolysin pore depends on the cation type: the alkali series probed by MD simulations and experiments. *J. Phys. Chem. C, Nanomater. Interfaces* **115**(10), 4255–4264 (2011)
20. Gu, L.Q., Dalla Serra, M., Vincent, J.B., Vigh, G., Cheley, S., Braha, O., Bayley, H.: Reversal of charge selectivity in transmembrane protein pores by using noncovalent molecular adapters. *Proc. Natl. Acad. Sci. U. S. A.* **97**(8), 3959–3964 (2000)
21. Gu, L.Q., Cheley, S., Bayley, H.: Prolonged residence time of a noncovalent molecular adapter, beta-cyclodextrin, within the lumen of mutant alpha-hemolysin pores. *J. Gen. Physiol.* **118**(5), 481–493 (2001)
22. de Groot, B.L., Grubmuller, H.: Water permeation across biological membranes: mechanism and dynamics of aquaporin-1 and GlpF. *Science* **294**(5550), 2353–2357 (2001)
23. Tajkhorshid, E., Nollert, P., Jensen, M.O., Miercke, L.J., O'Connell, J., Stroud, R.M., Schulten, K.: Control of the selectivity of the aquaporin water channel family by global orientational tuning. *Science* **296**(5567), 525–530 (2002)
24. Zhu, F., Tajkhorshid, E., Schulten, K.: Theory and simulation of water permeation in aquaporin-1. *Biophys. J.* **86**(1 Pt 1), 50–57 (2004)
25. Hummer, G., Rasaiah, J.C., Noworyta, J.P.: Water conduction through the hydrophobic channel of a carbon nanotube. *Nature* **414**(6860), 188–190 (2001)
26. Beckstein, O., Sansom, M.S.: Liquid-vapor oscillations of water in hydrophobic nanopores. *Proc. Natl. Acad. Sci. U. S. A.* **100**(12), 7063–7068 (2003)
27. Kalra, A., Garde, S., Hummer, G.: Osmotic water transport through carbon nanotube membranes. *Proc. Natl. Acad. Sci. U. S. A.* **100**(18), 10175–10180 (2003)
28. Joseph, S., Aluru, N.R.: Why are carbon nanotubes fast transporters of water? *Nano Lett.* **8**(2), 452–458 (2008)
29. Cisse, I., Okumus, B., Joo, C., Ha, T.J.: Fueling protein–DNA interactions inside porous nanocontainers. *Proc. Natl. Acad. Sci. U. S. A.* **104**(31), 12646–12650 (2007)
30. Holt, J.K., Park, H.G., Wang, Y.M., Stadermann, M., Artyukhin, A.B., Grigoriopoulos, C.P., Noy, A., Bakajin, O.: Fast mass transport through sub-2-nanometer carbon nanotubes. *Science* **312**(5776), 1034–1037 (2006)
31. Bonthuis, D.J., Horinek, D., Bocquet, L., Netz, R.R.: Electrohydraulic power conversion in planar nanochannels. *Phys. Rev. Lett.* **103**, 144503 (2009)
32. Joseph, S., Aluru, N.R.: Pumping of confined water in carbon nanotubes by rotation-translation coupling. *Phys. Rev. Lett.* **101**(6), 064502 (2008)
33. Tieleman, D.P., Hess, B., Sansom, M.S.P.: Analysis and evaluation of channel models: simulations of alamethicin. *Biophys. J.* **83**(5), 2393–2407 (2002)
34. Ni, B., Baumketner, A.: Effect of atom- and group-based truncations on biomolecules simulated with reaction-field electrostatics. *J. Mol. Model.* **17**(11), 2883–2893 (2011)
35. Wong-Ekkabut, J., Miettinen, M.S., Dias, C., Karttunen, M.: Static charges cannot drive a continuous flow of water molecules through a carbon nanotube. *Nature Nanotechnol.* **5**(8), 555–557 (2010)
36. Gong, X.J., Li, J.Y., Lu, H.J., Wan, R.Z., Li, J.C., Hu, J., Fang, H.P.: A charge-driven molecular water pump. *Nature Nanotechnol.* **2**(11), 709–712 (2007)
37. Berger, O., Edholm, O., Jahnig, F.: Molecular dynamics simulations of a fluid bilayer of dipalmitoylphosphatidylcholine at full hydration, constant pressure, and constant temperature. *Biophys. J.* **72**(5), 2002–2013 (1997)
38. Bernstein, F.C., Koetzle, T.F., Williams, G.J.B., Meyer, E.F., Brice, M.D., Rodgers, J.R., Kennard, O., Shimanouchi, T., Tasumi, M.: Protein Data Bank: computer-based archival file for macromolecular structures. *J. Mol. Biol.* **112**(3), 535–542 (1977)
39. Oostenbrink, C., Villa, A., Mark, A.E., Van Gunsteren, W.F.: A biomolecular force field based on the free enthalpy of hydration and solvation: the GROMOS force-field parameter sets 53A5 and 53A6. *J. Comput. Chem.* **25**(13), 1656–1676 (2004)
40. Kasianowicz, J.J., Misakian, M.: Electrostatic influence on ion transport through the alpha HL channel. *J. Membr. Biol.* **195**(3), 137–146 (2003)
41. Tieleman, D.P., Berendsen, H.J.C.: Molecular dynamics simulations of a fully hydrated dipalmitoyl phosphatidylcholine bilayer with different macroscopic boundary conditions and parameters. *J. Chem. Phys.* **105**(11), 4871–4880 (1996)
42. Bachar, M., Brunelle, P., Tieleman, D.P., Rauk, A.: Molecular dynamics simulation of a polyunsaturated lipid bilayer susceptible to lipid peroxidation. *J. Phys. Chem. B* **108**(22), 7170–7179 (2004)
43. Martinez-Seara, H., Rog, T., Karttunen, M., Reigada, R., Vattulainen, I.: Influence of cis double-bond parametrization on lipid membrane properties: how seemingly insignificant details in force-field change even qualitative trends. *J. Chem. Phys.* **129**(10), 105103 (2008)

44. Berendsen, H.J.C., Postma, J.P.M., van Gunsteren, W.F., Hermans, J.: Interaction models for water in relation to protein hydration. In: Pullman, B. (ed.) *Intermolecular Forces*, pp. 331–342. D. Reidel, Dordrecht (1981)
45. Hess, B., Kutzner, C., van der Spoel, D., Lindahl, E.: GROMACS 4: Algorithms for highly efficient, load-balanced, and scalable molecular simulation. *J. Chem. Theor. Comput.* **4**(3), 435–447 (2008)
46. Bussi, G., Donadio, D., Parrinello, M.: Canonical sampling through velocity rescaling. *J. Chem. Phys.* **126**(1), 014101 (2007)
47. Bussi, G., Zykova-Timan, T., Parrinello, M.: Isothermal-isobaric molecular dynamics using stochastic velocity rescaling. *J. Chem. Phys.* **130**(7), 074101 (2009)
48. Essmann, U., Perera, L., Berkowitz, M.L., Darden, T., Lee, H., Pedersen, L.G.: A smooth particle mesh Ewald method. *J. Chem. Phys.* **103**(19), 8577–8593 (1995)
49. Darden, T., York, D., Pedersen, L.: Particle mesh Ewald: an N.Log(N) method for Ewald sums in large systems. *J. Chem. Phys.* **98**(12), 10089–10092 (1993)
50. Karttunen, M., Rottler, J., Vattulainen, I., Sagui, C.: Electrostatics in biomolecular simulations: where are we now and where are we heading? *Comput. Model. Membr. Bilayers* **60**, 49–89 (2008). doi:10.1016/S1063-5823(08)00002-1
51. Humphrey, W., Dalke, A., Schulten, K.: VMD: visual molecular dynamics. *J. Mol. Graph.* **14**(1), 33–38 (1996)
52. Borgnia, M.J., Agre, P.: Reconstitution and functional comparison of purified GlpF and AqpZ, the glycerol and water channels from *Escherichia coli*. *Proc. Natl. Acad. Sci. U. S. A.* **98**(5), 2888–2893 (2001)
53. Paula, S., Akesson, M., Deamer, D.: Water transport by the bacterial channel alpha-hemolysin. *Biochim. Biophys. Acta-Biomembranes* **1418**(1), 117–126 (1999)
54. Yeh, I.C., Hummer, G.: Diffusion and electrophoretic mobility of single-stranded RNA from molecular dynamics simulations. *Biophys. J.* **86**(2), 681–689 (2004)
55. Guillot, B.: A reappraisal of what we have learnt during three decades of computer simulations on water. *J. Mol. Liq.* **101**(1-3), 219–260 (2002)
56. Abascal, J.L.F., Vega, C.: A general purpose model for the condensed phases of water: TIP4P/2005. *J. Chem. Phys.* **123**(23), (2005)
57. Patra, M., Karttunen, M.: Systematic comparison of force fields for microscopic simulations of NaCl in aqueous solutions: diffusion, free energy of hydration, and structural properties. *J. Comput. Chem.* **25**(5), 678–689 (2004)
58. Zeidel, M.L., Ambudkar, S.V., Smith, B.L., Agre, P.: Reconstitution of functional water channels in liposomes containing purified red cell CHIP28 protein. *Biochemistry* **31**(33), 7436–7440 (1992)
59. Yang, B., Verkman, A.S.: Water and glycerol permeabilities of aquaporins 1–5 and MIP determined quantitatively by expression of epitope-tagged constructs in *Xenopus* oocytes. *J. Biol. Chem.* **272**(26), 16140–16146 (1997)
60. Saparov, S.M., Antonenko, Y.N., Koeppe II, R.E., Pohl, P.: Desformylgramicidin: a model channel with an extremely high water permeability. *Biophys. J.* **79**(5), 2526–2534 (2000)
61. Saparov, S.M., Pohl, P.: Beyond the diffusion limit: water flow through the empty bacterial potassium channel. *Proc. Natl. Acad. Sci. U. S. A.* **101**, 4805–4809 (2004)
62. Doyle, D.A., Cabral, J.M., Pfuetzner, R.A., Kuo, A., Gulbis, J.M., Cohen, S.L., Chait, B.T., MacKinnon, R.: The structure of the potassium channel: molecular basis of K<sup>+</sup> conduction and selectivity. *Science* **280**(5360), 69–77 (1998)
63. MacKinnon, R., Cohen, S.L., Kuo, A., Lee, A., Chait, B.T.: Structural conservation in prokaryotic and eukaryotic potassium channels. *Science* **280**(5360), 106–109 (1998)
64. Zhu, F.Q., Schulten, K.: Water and proton conduction through carbon nanotubes as models for biological channels. *Biophys. J.* **85**(1), 236–244 (2003)
65. Beckstein, O., Biggin, P.C., Sansom, M.S.P.: A hydrophobic gating mechanism for nanopores. *J. Phys. Chem. B* **105**(51), 12902–12905 (2001)
66. Beckstein, O., Sansom, M.S.P.: The influence of geometry, surface character, and flexibility on the permeation of ions and water through biological pores. *Phys. Biol.* **1**(1-2), 42–52 (2004)
67. Zhu, F.Q., Tajkhorshid, E., Schulten, K.: Collective diffusion model for water permeation through microscopic channels. *Phys. Rev. Lett.* **93**(22), 238102 (2004)
68. Redner, S.: *A Guide to First-Passage Processes*. Cambridge University Press, (2001)
69. van Hijkoop, V.J., Dammers, A.J., Malek, K., Coppens, M.O.: Water diffusion through a membrane protein channel: a first passage time approach. *J. Chem. Phys.* **127**(8), 085101 (2007)
70. Coppens, M.O., Dammers, A.J.: Effects of heterogeneity on diffusion in nanopores—from inorganic materials to protein crystals and ion channels. *Fluid Phase Equilibria* **241**(1-2), 308–316 (2006)
71. Mashl, R.J., Joseph, S., Aluru, N.R., Jakobsson, E.: Anomalously immobilized water: a new water phase induced by confinement in nanotubes. *Nano Lett.* **3**(5), 589–592 (2003)

72. Feenstra, K.A., Hess, B., Berendsen, H.J.C.: Improving efficiency of large time-scale molecular dynamics simulations of hydrogen-rich systems. *J. Comput. Chem.* **20**(8), 786–798 (1999)
73. van der Spoel, D., van Maaren, P.J., Berendsen, H.J.C.: A systematic study of water models for molecular simulation: derivation of water models optimized for use with a reaction field. *J. Chem. Phys.* **108**(24), 10220–10230 (1998)
74. Striolo, A.: The mechanism of water diffusion in narrow carbon nanotubes. *Nano Lett.* **6**(4), 633–639 (2006)
75. Mukherjee, B., Maiti, P.K., Dasgupta, C., Sood, A.K.: Strong correlations and Fickian water diffusion in narrow carbon nanotubes. *J. Chem. Phys.* **126**(12), 124704 (2007)
76. Pellegrini, M., Gronbech-Jensen, N., Doniach, S.: Potentials of mean force for biomolecular simulations: theory and test on alanine dipeptide. *J. Chem. Phys.* **104**(21), 8639–8648 (1996)
77. Marrink, S.J., Berendsen, H.J.C.: Simulation of water transport through a lipid membrane. *J. Phys. Chem.* **98**(15), 4155–4168 (1994)
78. Marrink, S.J., Berendsen, H.J.C.: Permeation process of small molecules across lipid membranes studied by molecular dynamics simulations. *J. Phys. Chem.* **100**(41), 16729–16738 (1996)
79. Zuo, G., Shen, R., Ma, S., Guo, W.: Transport properties of single-file water molecules inside a carbon nanotube biomimicking water channel. *ACS Nano* **4**(1), 205–210 (2010)
80. Jorgensen, W.L., Jenson, C.: Temperature dependence of TIP3P, SPC, and TIP4P water from NPT Monte Carlo simulations: seeking temperatures of maximum density. *J. Comput. Chem.* **19**(10), 1179–1186 (1998)
81. Vega, C., Abascal, J.L.F.: Simulating water with rigid non-polarizable models: a general perspective. *Phys. Chem. Chem. Phys.* **13**(44), 19663–19688 (2011)
82. Shirts, M.R., Pitner, J.W., Swope, W.C., Pande, V.S.: Extremely precise free energy calculations of amino acid side chain analogs: comparison of common molecular mechanics force fields for proteins. *J. Chem. Phys.* **119**(11), 5740–5761 (2003)
83. Wanunu, M.: Nanopores: past, present and future. *Phys. Life Rev.* **9**(2), 174–176 (2012)
84. Braha, O., Walker, B., Cheley, S., Kasianowicz, J.J., Song, L.Z., Gouaux, J.E., Bayley, H.: Designed protein pores as components for biosensors. *Chem. Biol.* **4**(7), 497–505 (1997)
85. Bayley, H., Braha, O., Gu, L.Q.: Stochastic sensing with protein pores. *Adv. Mater.* **12**(2), 139–142 (2000)
86. Mathe, J., Aksimentiev, A., Nelson, D.R., Schulten, K., Meller, A.: Orientation discrimination of single-stranded DNA inside the alpha-hemolysin membrane channel. *Proc. Natl. Acad. Sci. U. S. A.* **102**(35), 12377–12382 (2005)
87. Ayub, M., Hardwick, S.W., Luisi, B.F., Bayley, H.: Nanopore-based identification of individual nucleotides for direct RNA sequencing. *Nano Lett.* **13**(12), 6144–6150 (2013)
88. Maffeo, C., Bhattacharya, S., Yoo, J., Wells, D., Aksimentiev, A.: Modeling and simulation of ion channels. *Chem. Rev.* **112**(12), 6250–6284 (2012)